Surface active fatty acid ILs: influence of the hydrophobic tail and/or the imidazolium hydroxyl functionalization on aggregates formation

Andrea Mezzetta,[a] Justyna Łuczak,[b] Julia Woch,[c] Cinzia Chiappe,[a] Janusz Nowicki,[c,*] Lorenzo Guazzelli[a,*]

[a]Department of Pharmacy, University of Pisa, Via Bonanno 33, 56126, Pisa, Italy

[b]Department of Process Engineering and Chemical Technology, Chemical Faculty, Gdansk University of Technology, Narutowicza 11/12, 80-233 Gdansk, Poland

[c]Department of Renewable Raw-Materials Processing, Institute of Heavy Organic Synthesis "Blachownia", Energetyków 9, 47-225 Kędzierzyn-Koźle, Poland

Abstract

Nine structurally-related fatty acid ionic liquids have been prepared and their thermal behavior as well as their ability to self-assemble in water has been investigated. The thermal properties were studied by thermal gravimetric analysis (TGA) and differential scanning calorimetry (DSC), while the aggregation behavior was analyzed by tensiometry, isothermal titration calorimetry (ITC), conductometry, dynamic light scattering (DLS), and electrophoretic light scattering (ELS). Structural variations concerned both the imidazolium cation (presence or not of hydroxyl groups) and the anion (length of the fatty acid), and affected in different ways the ILs' properties.

With regards to the thermal stability, the presence of the hydroxyl group on the cation had a beneficial effect on stability regardless of the anion's length. This latter played instead a major role in allowing the solubility of the ILs in water (C18-stearate ILs were not soluble in water) and in determining the critical micelle concentration (CMC) values, as the reduction of the anion length in moving from C16-palmitate to C14-myristate anions disfavors aggregates formation.

Several other parameters characterizing the adsorption of fatty acid ILs at the air/water interface, some thermodynamic parameters of the aggregation process as well as size distribution and stability of the aggregates were also determined.

1. Introduction

Ionic liquids (ILs) are organic salts constituted by an organic cation and an organic or an inorganic anion. Although salts, the way the cation and the anion are arranged in the ionic structure can lead to low melting points for these structures. Usually, organic salts that are liquid at a temperature lower than 100 °C are considered ILs with full rights. However, there is no scientific justification to this arbitrary classification, which was probably introduced to draw a line between ILs and high temperature inorganic molten salts [1]. Other physico-chemical properties, which are remarkable for organic compounds, such as for instance the high thermal stability, negligible vapor pressure, low flammability and wide electrochemical window suggested the possibility to replace traditional volatile organic solvents (VOCs) with these media [2]. Although nowadays it is known that ILs are not green and safe by nature and care should always be paid on the environmental impact of their preparation [3] and on their toxicity [4], nevertheless, the area of interest and the applications of ILs are continuously expanding. ILs are widely studied for instance in organic synthesis, [5] biopolymers dissolution, transformation and recycling, [6-13] electrochemistry applications [14], biosensor development [15,16], and as new potential agrochemicals [17,18].

One of the most impressive features of ILs lies in the possibility to combine an almost limitless number of known ions. Hence, their properties can be finely tuned on whatever problem needs to be addressed. In this context, a peculiar option stands in the possibility to further tailor their structure by inserting additional functional groups, mostly on the cation, which gives rise to the so called class of task-specific ILs [19]. The introduction of for instance hydroxyl, amino or carboxyl groups has an effect both on the physico-chemical properties of ILs and on their ability to address specific challenging issues.

However, Bara *et al* [20] showed that the understanding of the relationship between ILs structures and their properties is clearly still limited. Moreover, even if the most studied 1,3-dialkyl imidazolium cation are considered, only 5% of the possible structures are present in the literature.

Analysis of the structure-activity relationship of ILs revealed that their chemical composition, namely the presence of charged hydrophilic headgroup and hydrophobic alkyl substituent, resembles that of the conventional cationic surfactants. This characteristic structure determines the amphiphilic properties, thus the ability to self-assembly in aqueous solutions into a variety of structures such as micelles, vesicles, lamellas and membranes [21-23]. The lower critical micelle concentration (CMC) is the lower amount of ILs needed to form micelles, and IL's structural elements facilitating aggregation at lower concentration have been the object of intense investigation. In this regard, the length and number of alkyl substituents in the cation [22], the type

of the hydrophilic headgroup [24], the nature of the counter ion [25], the effect of the temperature [26] and presence of additional compounds in the micellar environment [27] were all examined. It was found, among other, that micelles of ILs are formed at lower CMC values in comparison with cationic surfactants with similar structures [28]. In the mentioned research, the most intensively studied ILs were long alkyl chain imidazolium derivatives, where halogens were used as counter ions. ILs were usually employed as cationic amphiphiles since hydrophobic alkyl substituents were located at the cation moiety. However, up to this date, modification of the ILs structure toward the ability to form anionic aggregates was scarcely investigated.

The ability of amphiphilic compounds to self-assemble affects many chemical and biotechnological processes and is also significant from the environmental perspective. Therefore, understanding the micellization behavior of ILs in aqueous solution is a vital part of predicting, controlling, and designing their properties and finally their applications. In this regard, the IL micellar systems were studied in various areas such as nanomaterials formation [29], organic synthesis [30], micellar catalysis [31], micellar extraction [32, 33], drug delivery [34], and antimicrobial activity [25, 35].

A late trend in the ILs research area is to study the replacement of petrol derived components with natural or bio-based compounds [36]. In this context, quite recently, fatty acids have attracted increasing interest and have been studied as potential anion both for classical ILs and for protic ILs. Several different aspects of fatty acid-based ILs have been investigated such as their synthesis, with the aim to reduce to a minimum the use of organic solvents thus lowering the environmental impact of their preparation [37-39], their applications as bio-lubricants/bio-lubricants additives [40-42] or as potential media for the separation of butene and butadiene [43]. Furthermore, lately, the phase behavior and aggregation phenomena in water of fatty acid ILs have been a topic of intense study [39, 44-47].

In this work, we present an investigation on the properties of nine fatty acid ionic liquids characterized by structural variation both on the cation (presence or not of a hydroxyl group) and on the hydrophobic anion (different length of the fatty acid used). The prepared ILs have been characterized by NMR, FTIR, TGA and DSC. Furthermore the aggregation behavior of the prepared ILs in water has been investigated using tensiometry, isothermal titration calorimetry (ITC), conductometry, and dynamic light scattering (DLS).

2. Experimental

2.1. Materials

1-Ethyl-3-methylimidazolium [EMIM] methylcarbonate methanol solutions (30% m/m, 99%) was purchased from Proionic GmbH. Myristic acid (99%), palmitic acid (≥99%), and stearic acid (95%), were obtained from Sigma-Aldrich. 1-Methylimidazole, 2-chloroethanol, and 3-chloropropanol were purchased from Sigma-Aldrich. All reagents were used as received, without further purification.

The synthesis of fatty-acid ILs **1-9** was based on a neutralization reaction. However, due to the diverse nature of the anions of the starting ILs (Figure 1), two different procedures were followed (please refer to the supporting information file for experimental details). EMIM based ILs **1-3** were prepared from the commercial methyl carbonate IL precursor by following a previously reported method approach developed by some of us [37]. Briefly, an equimolar amount of the selected fatty acid was added to the methanolic solution of EMIM methyl carbonate and the reaction mixture was heated to 40 °C. Soon after the addition of the acid, the decomposition of the methyl carbonate into CO_2 and methanol was noticeable from the gas evolution. At the end of the reaction (1 hour), the solvent was removed under vacuum to afford the target structure in a quantitative yield. The preparation of ILs **4-9** required a well-known two steps procedure. The hydroxyl functionalized chloride ILs [48] were first converted into the corresponding hydroxides by passing them through an anion exchange resin [49], neutralized by corresponding fatty acids and carefully purified [50]. The structures of ILs **1-9** are summarized in Table 1.

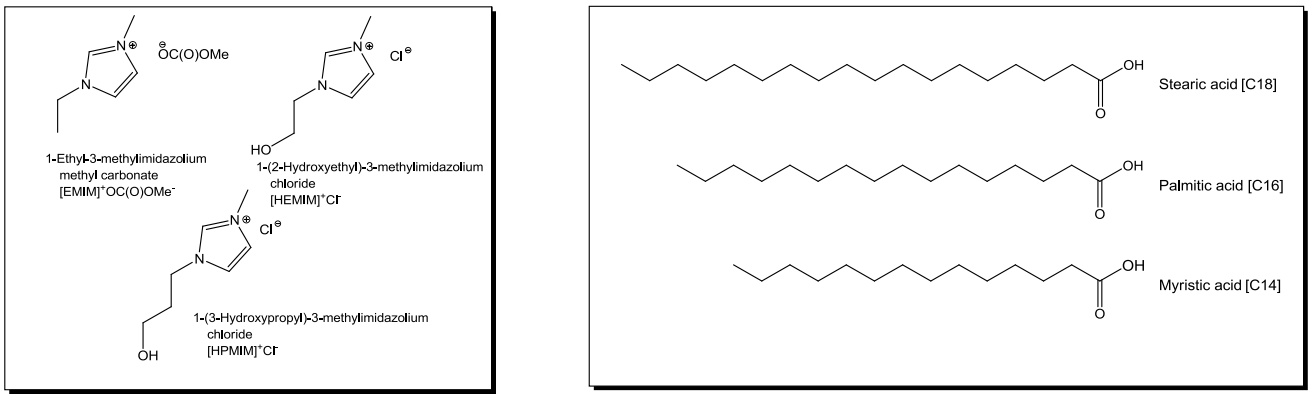

Figure 1. ILs precursors (left side) and fatty acids (right side) used for the preparation of target ILs.

LCFA-IL	Cation	Anion
1	[EMIM]	Myristate [C14]
2[a]	[EMIM]	Palmitate [C16]
3[a]	[EMIM]	Stearate [C18]
4	[HEMIM]	Myristate [C14]

5	[HEMIM]	Palmitate [C16]
6	[HEMIM]	Stearate [C18]
7	[HPMIM]	Myristate [C14]
8	[HPMIM]	Palmitate [C16]
9	[HPMIM]	Stearate [C18]

[a] Fatty acid ILs **2** and **3** have been reported in [37].

Table 1. Fatty acid ILs prepared in the present study.

2.2. Analytical and physico-chemical methods

NMR spectra

NMR spectra were recorded at room temperature using a Bruker Instrument at 250.13 MHz (^{1}H) and 62.9 MHz (^{13}C) using deuterated chloroform as solvent. The following abbreviations are used: s=singlet, m=multiplet, bs=broad singlet, t=triplet, bt=broad triplet, q=quartet, qui= quintuplet, sext=sextet. Infrared spectra were registered using an ATR-FTIR Agilent 660 with diamond crystal (Agilent Technologies, Santa Clara, CA, USA).

Thermogravimetric analysis and differential scanning calorimetry

Prior to thermogravimetric analysis (TGA) and differential scanning calorimetry (DSC) measurement, all samples were dried in high vacuum at 60 °C for 24 hours, to remove moisture and any volatile materials.

The thermal stability of the synthesized ILs was investigated by TGA analysis, conducted in a TA Instruments Q500 TGA. For weight calibration, weight standards were used (1 g, 500 mg and 100 mg). The temperature calibration was performed using nickel standard. All the standards were supplied by TA Instruments Inc. The sample (15-20 mg) was heated in a platinum crucible as sample holder. For the drying procedure the IL was maintained at 60 °C in N_2 flux (90 mL/min) for 30 min. Then, IL was heated from 40 °C to 500 °C with a heating rate of 10 °C/min under nitrogen (90 mL/min) and maintained at 500 °C for 3 min. Mass change was recorded as a function of temperature and time. TGA experiments were carried out in triplicate.

The thermal behavior of the ionic liquids was analyzed by using a differential scanning calorimeter (TA DSC, Q250, USA). The temperature calibration was performed considering the heating rate dependence of the onset temperature of the melting peak of indium. Dry high purity N_2 gas with a flow rate of 30 mL/min was purged through the sample. In order to allow volatile compounds to escape and to avoid the risk of the pan bursting under pressure, a small incision was made in the top

of both the sample and the reference pan. The sample (5-8 mg) was loaded in hermetic aluminum crucibles and dried at 130 °C for 30 min. Then, the phase behavior was explored under nitrogen atmosphere in the temperature range of -90 to 100 °C with a heating rate of 2 °C/min. DSC experiments were carried out in duplicate.

T_g was obtained by taking the onset of the heat capacity change on heating from a glass to a liquid. T_{cc} was determined as the peak temperature of the exothermic peak on heating from subcooled liquid to a crystalline solid. T_m was taken as the peak temperature of the endothermic peak under heating conditions. The peak temperatures were chosen instead of the onset temperatures due to the complexity of the DSC curve.

Surface tension measurements

A video based optical contact angle meter (OCA 15, Dataphysics) was used for the surface tension isotherms determination of the IL solutions at 25±0.1 °C. The SCA 22 software module enabled the measurement of surface tension according to the pendant drop. The temperature of the samples was controlled by a thermostatic water bath (PolyScience, AD07R-20).

Based on the surface tension measurements the maximum surface excess concentration, Γ_{max}, and the minimum area per IL surfactant molecule, Amin, at the air/water interface were calculated according to the following equations:

$$\Gamma_{max} = -\frac{1}{RT}\left[\frac{d\gamma}{d\ln c}\right]_{T,p} \quad (1.\ 1)$$

$$\boldsymbol{A_{min}} = \frac{\boldsymbol{10^{16}}}{\boldsymbol{N_A \cdot \Gamma_{max}}} \quad (1.\ 2)$$

where R is the gas constant, T is the absolute temperature, γ is surface tension [mN/m], c is the concentration of IL in the solution [mmol/L], and N_A is the Avogadro constant. The efficiency of adsorption of the amphiphiles at the air/water interface (pC20) was determined as the negative logarithm of the amphiphile concentration required to reduce the surface tension of water by 20 mN/m. The surface pressure (the surface tension reduction effectiveness) at the CMC, Π_{cmc}, was obtained by means of equation (1. 3):

$$\boldsymbol{\Pi_{CMC} = \gamma_o - \gamma_{CMC}} \quad (1.\ 4)$$

where γ_o is the surface tension of the solvent and γ_{CMC} is the surface tension at CMC.

Conductivity measurements

The conductivity measurements were performed using a conductivity meter equipped with an autotitrator (Cerko Lab System CLS/M/07/06, Poland), a microelectrode (Eurosensor, EPST-2ZA,

Poland) and a thermostatic water bath (PolyScience 9106, USA). Temperature measurement accuracy remained within ±0.1 °C. The conductivity cell constant *k* was determined with a range of aqueous solutions of KCl (0.1–100 mmol/L). The degree of ionization of the micelles (β) was calculated from the ratio of the dκ/dc slopes of the two linear fragments of the conductivity curves.

Isothermal titration calorimetry (ITC)

The thermodynamic parameters of the micellization process were determined with Nano-Isothermal Titration Calorimeter III (N-ITC III, CSC, USA). The sample and reference cells were filled with water whereas the syringe was loaded with the IL solution with a concentration about ten times higher than the expected CMC to observe the demicellization process. The titration experiment consisted of 48 injections of 5.15 μL of IL aliquots. The enthalpograms were created using Titration Bindworks software. The enthalpy of demicellization (ΔH_{dm}) and CMC value were determined from the enthalpograms.

The free energy of the micellization process was calculated using equation (1. 5):

$$\Delta G_m = (2 - \beta) RT ln X_{CMC} \quad (1.\ 6)$$

where β is the degree of ionization taken from conductivity measurements and X_{CMC} is the mole fraction of the IL monomers at critical micelle concentration. The free energy of the micellization was calculated using average CMC taken from three methods. The entropy of micellization, ΔS_m, was obtained from the relationship as given in equation (1. 7):

$$\Delta \boldsymbol{S_m} = \frac{\mathbf{1}}{\boldsymbol{T}} (\Delta \boldsymbol{H_m} - \Delta \boldsymbol{G_m}) \quad (1.\ 5)$$

Dynamic light scattering (DLS)

The size and dispersity of the aggregates formed in solution by studied ILs were determined by dynamic light scattering (DLS) using Zetasizer Nano ZS analyser with vertically polarised incident light of wavelength λ = 633 nm. All measurements were carried out at an angle of 173°. The autocorrelation functions were analysed with the algorithm CONTIN. The apparent hydrodynamic diameter of particles (D_h) was calculated using the Stokes–Einstein equation. The dispersity of particle sizes was given as $\frac{\mu_2}{\Gamma^2}$, where Γ is the average relaxation rate and μ_2 is its second moment, both values obtained by cumulant analysis.

The samples were prepared using ultrapure water (with conductivity = 0,05 μS/cm) obtained with Arium Mini Ultrapure water system (Sartorius). Before measurements, ILs solutions were filtered through Pureland PVDF syringe filters with nominal pore size 0.2 μm.

All measurements were carried out at concentration equals to 5 CMC and at 30 °C. For IL **1** and IL **4** the measurements were also performed at 25 °C. Hydrodynamic diameters were calculated according to equation1. 6:

$$D = \frac{kT}{3\pi\eta D_h} \quad (1.\,6)$$

Electrophoretic light scattering (ELS)

Zeta potential (ZP) measurements of the aggregates formed in solution were conducted using Zetasizer Nano ZS (Malvern) by electrophoretic light scattering. ZP was determined from electrophoretic mobility (μ) with the use of Smoluchowski approximation through equation 1. 7:

$$\mu = \frac{ZP\varepsilon mV}{a\pi\eta E} \quad (1.\,7)$$

where V is the applied voltage expressed in V, η is the viscosity of the solution, εm is the dielectric constant of the medium [Pa·s], and E is the electrode separation [m].

The samples (the same solutions as used for DLS) were measured at 30 °C. For IL **1** and IL **4** the measurements were also performed at 25 °C.

3. Results and discussion

NMR and FTIR analyses confirmed the identity of the prepared ILs. For what concern the FTIR spectra (please refer to the supplementary information file), distinct vibrational modes were discernable for methyl and methylene groups (stretching at 2917-2848 cm^{-1}, bending at 1466 cm^{-1} - 1360 cm^{-1}), the imidazolium cation (methyl bending at 1393 -1360 cm^{-1}, which overlaps with the symmetric stretching band of the carboxylate and the methyl-methylene bending, in-plane C_{Im} bending at 1181-1167 cm^{-1}) and the carboxylate group (asymmetric and symmetric stretching at 1560-1567 cm^{-1} and 1393-1360 cm^{-1} respectively).

3.1. Thermal analysis of prepared fatty acid ILs

The thermal stability of ILs **1-9** was evaluated by means of dynamic relative analysis. Although it is known [51] that this analysis overestimates the degradation temperature, it allows however for comparing the thermal stability of a series of compounds under identical conditions.

$T_{start,}$ T_{onset} and T_{peak} values are reported in Table 2 (average values of three temperature-ramped TGA experiments).

LCFA-IL	Cation	Anion	T_{start}	T_{onset}	T_{peak}
1	[EMIM]	Myristate [C14]	217	234	258
2	[EMIM]	Palmitate [C16]	224	238	263
3	[EMIM]	Stearate [C18]	227	242	268
4	[HEMIM]	Myristate [C14]	244	263	295
5	[HEMIM]	Palmitate [C16]	248	264	299
6	[HEMIM]	Stearate [C18]	248	259	284
7	[HPMIM]	Myristate [C14]	243	260	292
8	[HPMIM]	Palmitate [C16]	246	260	289
9	[HPMIM]	Stearate [C18]	250	261	288

Table 2. $T_{start,}$ T_{onset} and T_{peak} values for ILs **1-9** measured under a nitrogen atmosphere and with a heating rate of 10 °C/min.

In particular, the 10 °C/min heating rate was chosen for comparison purpose in order to permit a correlation of the T_{onset} values with the ILs stability levels reported by Cao and Mu [52]. For ILs **2** and **3**, higher T_{onset} values than the previously reported ones with the 5 °C/min heating rate [37] were recorded. This outcome is in agreement with the influence of the temperature scanning rate on the nonisothermal thermogravimetric results [53].

The hydroxyl functionalized ILs **4-9** displayed T_{onset} values in a very limited range (259-264 °C) no matter the length of the hydrophobic tail or the length of the imidazolium substituent. Conversely, EMIM ILs **1-3** showed lower T_{onset} values which increased by increasing the length of the fatty acid anion. From these data, it appears that the presence of a hydroxyl group on the cation determines an increase of the overall thermal stability of the ILs (Figure 2).

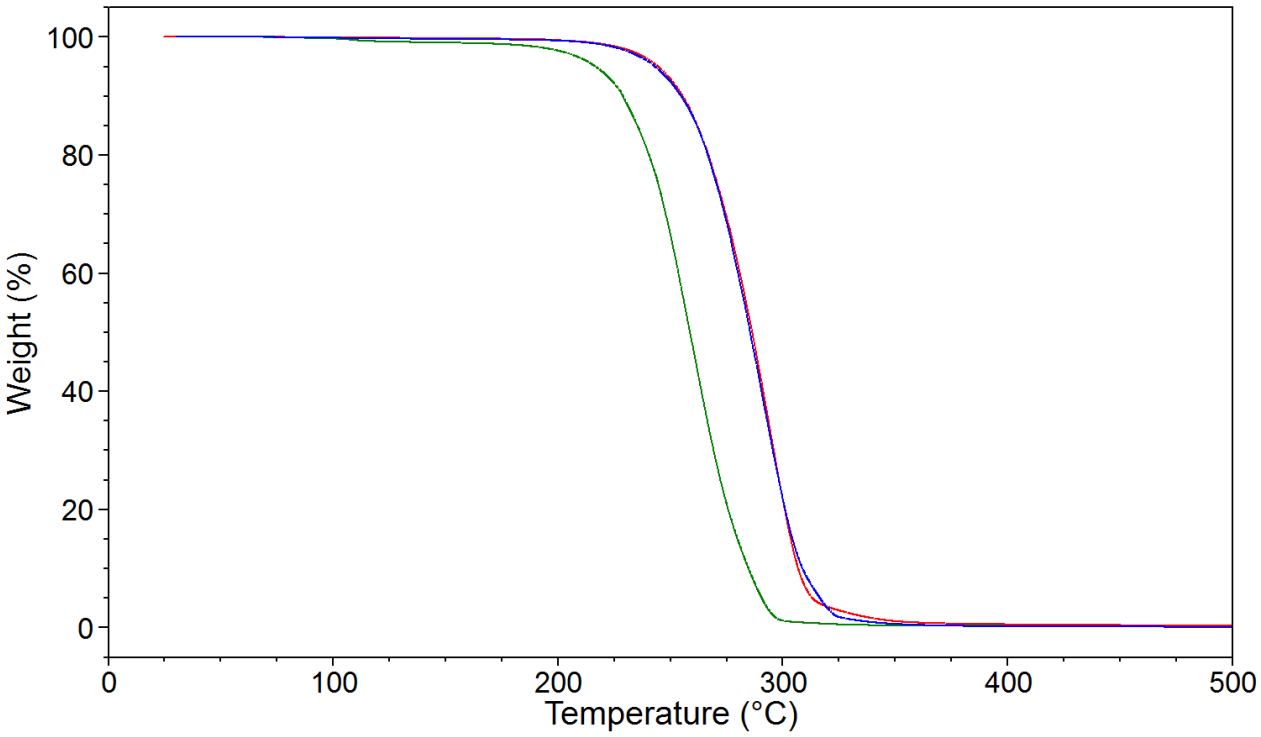

Figure 2. TG curves for Myristate ILs **1** (green line), **4** (red line) and **7** (blu line) with heating rate of 10 °C/min.

Although a reverse effect was observed in the case of a different anion (EMIM Tf_2N was more thermally stable than HEMIM Tf_2N [54]), for the analogous acetate ILs the same trend was highlighted before [52]. Therefore, the results here obtained strengthen the hypothesis that a hydrogen bond interaction between the carboxylate anion and the hydroxyl group on the cation takes place and is able to hinder the thermal decomposition to some extent.

When looking to the ILs stability classification mentioned above, [52] ILs **1**-**3** belong to the least stable level (200 °C < T_{onest}<250 °C), while the extra stabilization related to the functionalization of the imidazolium substituent places ILs **4**-**9** within the less stable level (250 °C < T_{onest}<300 °C).

Thermal behaviors were investigated by differential scanning calorimetry at 2 °C/min in nitrogen flow in the temperature range going from -90 °C to 100 °C. Usually, three different behaviours are observed for ILs, which present either only glass transitions in the experiments under cooling and heating modes (type I), or a crystallization during the cooling half cycle and the corresponding melting during the heating half cycle, similar to a low melting salt (type II), or cold crystallization and melting both during the heating run (type III) [55].

For this set of ILs, a far more complicated scenario of phase transitions was instead observed, which spanned from two crystallizations, a cold crystallization and a melting event in the case of **1** (Figure 3, top) to a glass transition, a crystallization, two overlapping cold crystallizations, and two melting

events for **4** (Figure 3, bottom, please refer to the supplementary information file for the other DSC thermograms). All phase transitions found for ILs **1-9** are summarized in Table 3.

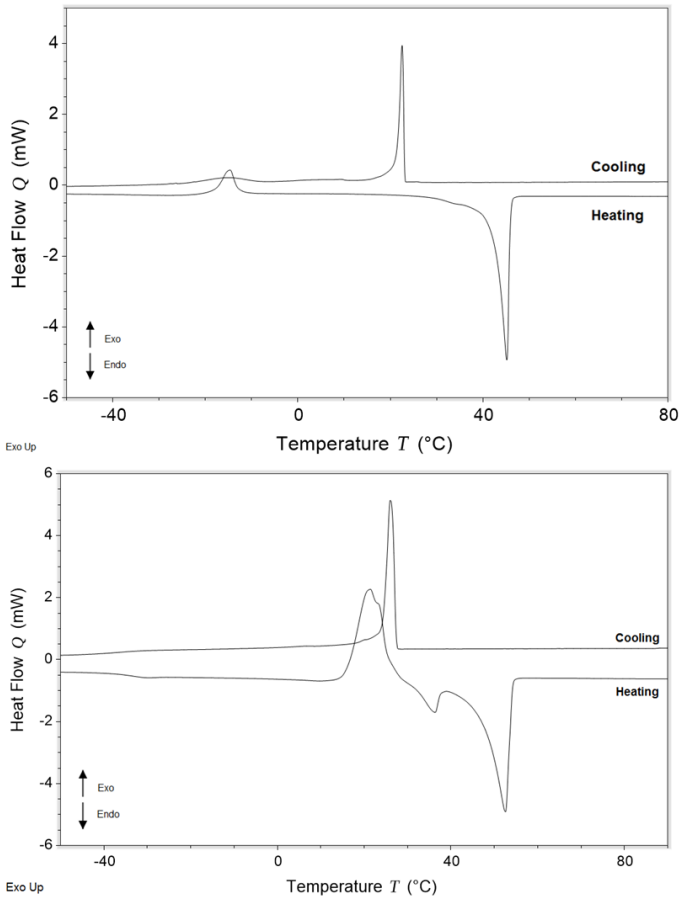

Figure 3. Differential scanning calorimetry (DSC) curves of compounds **1** [EMIM Myristate] (top) and **4** [HEMIM Myristate] (bottom)**.**

Cation	Anion	Temperature (°C)			
		Tg	Tc	Tcc	Tm
[EMIM]	[C14]	-	22.5 -15.5	-5.6	45.2
	[C16]	-35.5	43.2	2.9	49.1 53.7
	[C18]	-34.3	55.1	22.7	608
[HEMIM]	[C14]	-37.1	26.0	24.4	21.2 52.6
	[C16]	-30.3	45.4	42.0 50.0	62.4

	[C18]	-	47.3	49.7	66.3
[HPMIM]	[C14]	-	16.9	0.7 11.9	21.3 51.0
	[C16]	-37.5	38.6	30.6	42.7 58.2
	[C18]	-	49.3	42.5	52.7 65.6

Table 3. Glass transition (T_g), crystallization (T_c), cold crystallization (T_{cc}), and melting (T_m) temperatures for ILs **1**-**9**.

This kind of complex thermal behavior seems a distinct trait of fatty acid ILs [56] and is probably mostly related to the long hydrophobic anion as similar outcomes have been reported before with different cations [37,56].

The crystallization temperatures, which fall in a quite clean part of the DSC curves for all ILs, were compared to analyse possible correlations between this phase transition and the structural variations. For all ILs **1**-**9**, an increase of the T_c was observed by increasing the length of the anion, which reflects the melting point order of the fatty acids [myristic acid (C14) < palmitic acid (C16) < stearic acid (C18)] and is a consequence of more regular packing arrangements [44]. The T_c values when moving from the myristate anion to the palmitate anion are in line with previous finding which reported, for ILs based on the 1-butyl-3-methylimidazolium cation, an increase of 18 °C when the chain length of the carboxylate anion was increased by two carbon atoms [57]. Lower increases were instead observed in our case when the length of the anion was further elongated.

3.2. Aggregation behavior of studied ILs in water

The surface activity of six long chain fatty acid ILs with different hydrophobicity of the anion (myristate and palmitate) and with varied hydrophilicity of the cation (presence or not of a hydroxyl group) was investigated using surface tension and conductivity measurements (ILs **1**-**2**, **4**-**5**, and **7**-**8**). Solubility of stearate ILs **3**, **6** and **9** in aqueous solution was instead too low to perform these experiments. The surface tension isotherms of the fatty acids ILs solutions as a function of the increasing concentration of the solute in water are represented in Figure 4. The amphiphilic structure of the ILs determines their ability to adsorb at the air/water interface, to reduce the solution's surface tension when concentration increases, and to form the micellar aggregates after reaching CMC. Since aggregates are not surface active, surface tension of the solutions at concentrations above CMC is maintained at values approximately constant (plateau region in surface tension isotherms). The conductivity changes determined for the increasing concentration of

fatty acid ILs reflects the increasing number of ions in the aqueous solutions (Figure 5). The presence of a discontinuity in the trend is related to the formation of the aggregates and indicates the CMC of the compound. In this regard, two linear regions with different slopes were observed below and above the discontinuity indicating that the formed micelles have lower mobility in comparison with free IL ions (the lower slope after reaching CMC).

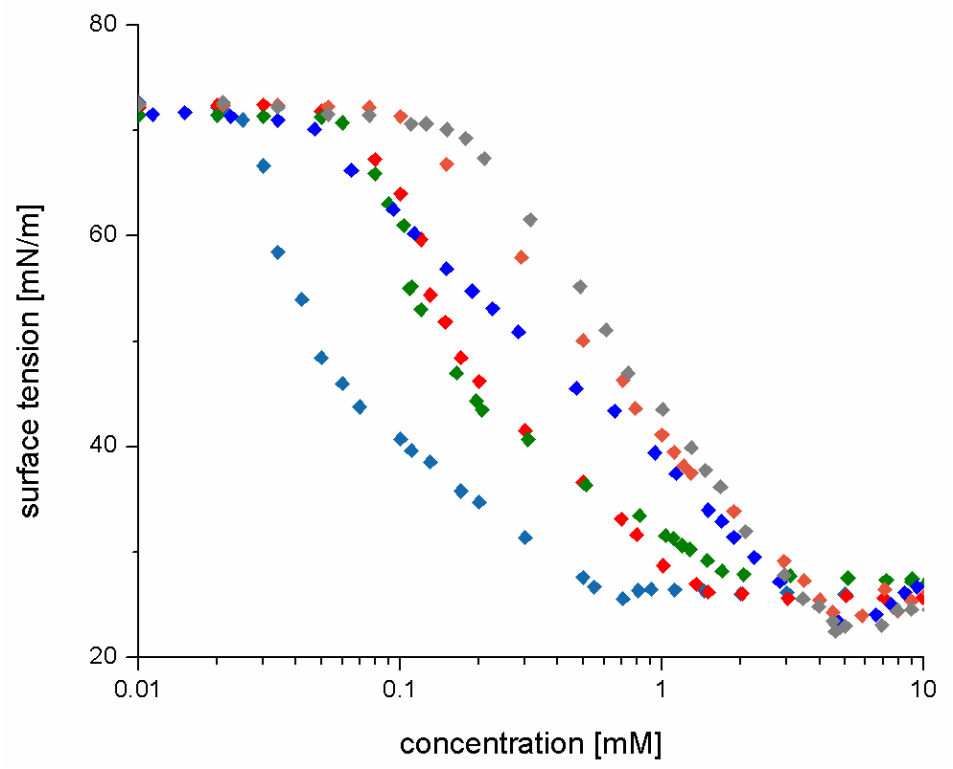

Figure 4. Surface tension (σ[mN/m]) data vs. IL concentration (c [mmol/L]) isotherms measured at 25 °C for aqueous solutions of **2** [EMIM Palmitate] (◆), **5** [HEMIM Palmitate] (◆), **8** [HPMIM Palmitate] (◆), **7** [HPMIM Myristate] (◆), **1** [EMIM Myristate] (◆), and **4** [HEMIM Myristate] (◆)

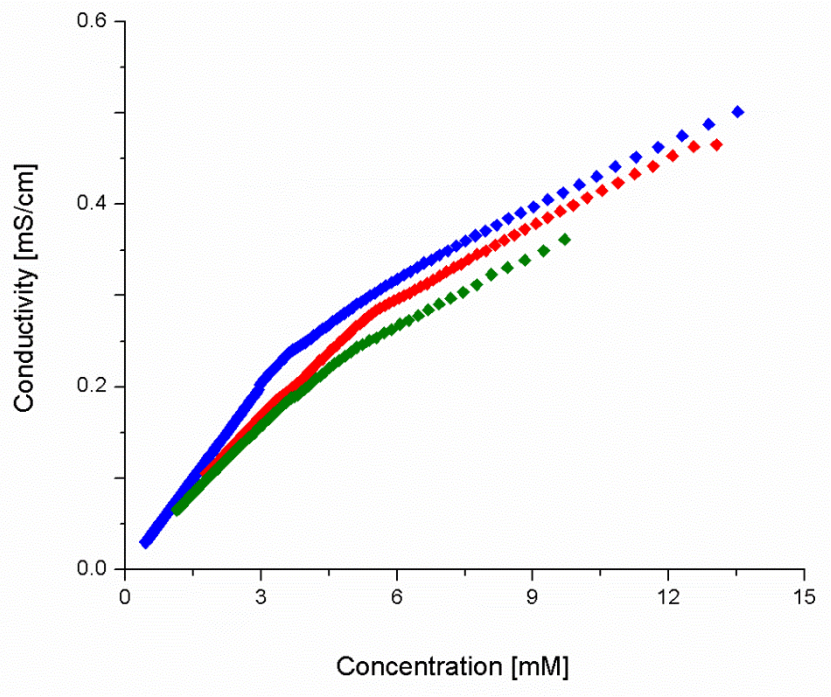

Figure 5. Exemplary results of specific conductivity (κ [mS/cm]) variation vs. concentration (c [mmol/L]) of **1** [EMIM Myristate] (◆), **4** [HEMIM Myristate] (◆) and **7** [HPMIM Myristate] (◆) in aqueous solutions at 25 °C

The data obtained by these two methods were further used for the calculation of the parameters characterizing adsorption of fatty acid ILs at the air/water interface (Γ_{max}, A_{min}, pC_{20}, Π_{cmc} and ΔG_{ad}), and micellization properties of the amphiphiles in aqueous solution (γ_{CMC}, CMC, β, ΔG_{mic}) using equations (1. 1) and (1. 3). These parameters are presented and compared in Table 4.

Generally, a reasonable agreement between these two CMC determination methods was observed. Self-aggregation of the amphiphile monomers involves a dynamic, association-dissociation equilibrium. Different physical properties that are measured and are influenced by the aggregates formation lie at the heart of the differences. The CMC values do not seem to be significantly influenced by the IL cation type but rather the anion structure. As it was expected, reduction of the chain length in the anion increases CMC, thus disfavoring micelle formation due to the lower hydrophobicity of the compound. For example, an increase of CMC from 0.7 to 4.0 mmol/L as determined by surface tension measurements for IL with [EMIM] cation was found when decreasing the number of the carbons atoms in the anion from C16 to C14. The addition of the hydroxyl group to the alkyl substituent of the imidazolium cation resulted in the similar effect, namely an increase of the CMC values but to a lower extent. The effect of the counterions on the micellization ability may be caused by many factors such as size, hydrophobicity, hydration and polarizability. In this regard, this behavior may be correlated with the higher hydrophilicity (thus

hydration) of the hydroxy derivatives ([HEMIM] and [HPMIM]) as well as the higher steric hindrance that may impede shielding of the negative charge on the carboxylic headgroups in the aggregate. As a consequence, the coulombic repulsion between the fatty acid IL headgroups is higher as reflected and confirmed by the increased ionization degree of the aggregate (Table 4). Thus, the higher the β value, the lower the degree of compactness of the aggregate. Analogously, the higher β value detected for ILs containing myristate [C14] anion (0.45-0.55) implies that less counterions are attracted to the surface layer of the aggregate in comparison with the palmitate one ([C16], 0.30-0.33). For comparison, CMCs of sodium palmitate and sodium myristate were found to be higher (2.1 mmol/L [58, 59] and 6.9 mmol/L [59], respectively), than the values determined for all fatty acids ILs in this study.

The lower number of water molecules in the hydration layer in comparison with Na^+, thus the higher hydrophobicity of the imidazolium cation, could be tentatively put forward as an explanation for the tendency of fatty acid ILs to aggregate at lower concentrations. The ability of fatty acid ILs to form aggregates were also found to be analogous to that of 1-alkyl-3-methylimidazolium chlorides [22], slightly higher than for 1-alkyl-3-methylimidazolium bromides [AMIM][Br] [60] and tetrafluoroborates [61] with the same alkyl chain length, however linked to the imidazolium cation (cationic amphiphiles).

Table 4. Summary of the surface properties of long chain fatty acid ionic liquids in aqueous solutions at 25 **°C**

LCFA-IL	CMC[a], mmol/L	CMC[b], mmol/L	β	pC_{20}	$\Gamma_m \cdot 10^6$, mol/m^2	A_m, nm^2	γ_{CMC}, mN/m	Π_{CMC}, mN/m	ΔG_{ad}, kJ/mol
[EMIM Myristate] 1	4.0	3.8	0.45	3.36	2.52	0.64	24.40	46.98	-55.3
[EMIM Palmitate] 2	0.7	1.3	0.30	4.36	1.76	0.91	25.60	47.09	-74.2
[HEMIM Myristate] 4	4.5	5.6	0.50	3.40	2.95	0.55	22.50	49.00	-54.8
[HEMIM Palmitate] 5	1.5	2.0	0.31	3.84	2.07	0.77	26.20	46.01	-66.3
[HPMIM Myristate] 6	4.7	4.7	0.55	3.59	2.05	0.79	23.44	48.48	-52.1
[HPMIM Palmitate] 7	1.7	2.1	0.33	3.89	1.45	1.11	28.20	43.76	-73.2

[a] surface tension

[b] conductivity

β, the degree of ionization; γ_{cmc}, the surface tension at the CMC; pC_{20}, the surfactant concentration required to reduce the surface tension of the solvent by 20 mN/m; Γ_{max}, the maximum surface excess concentration; A_m, the minimum area per molecule at the interface; Π_{cmc}, surface pressure at the CMC; ΔG_{ad}, free energy of adsorption..

The highest ability to form aggregates (the lowest CMC) was detected for 1-ethyl-3-methylimidazolium palmitate [EMIM palmitate], compound **2** (0.7 mmol/L). This ionic liquid was also characterized by the largest adsorption efficiency at the air/water interface (4.36). This may be caused by a tighter binding of the [EMIM] counterion to the aggregate. As it was expected, amphiphiles with less carbon atoms in their alkyl chain (myristates [C14]) revealed lower pC_{20} values, thus less efficiently adsorb at the interface and depress surface tension. The myristate ILs are also characterized by relatively higher maximum surface excess concentration, Γ_{max}, and correspondingly lower estimated area per IL ion pair at the air/water interface, A_{min}, indicating higher degree of packing (relatively more perpendicular orientation) at the air/water interface when compared with palmitate [C16] analogues. It was observed that Γ_{max} and pC_{20} parameters do no follow the same trend, namely significant lowering of the surface tension at low concentrations (higher pC_{20}, more efficient IL) is accompanied by lower Γ_{max} (less effective salt). Similar observations were previously made for many surfactants [62] since surface access is related to the amphiphile structure of the compound whereas pC_{20} to the free energy change associated with the transfer of the compound from the bulk phase to the interface.

The values of surface tension at CMC, γ_{CMC}, were found to be close to 23-28 mN/m, thus the effectiveness of fatty acids ILs in reducing surface tension, represented by the maximum reduction obtained regardless of the IL's concentration (surface pressure), was found to be in the range of 44-49 mN/m. These observations highlight the very high effectiveness of fatty acid ILs in reducing surface tension. In comparison, γ_{CMC} for cationic ILs amphiphiles [60, 63] was found to be much higher (34-42 mN/m), whereas values observed for nonionic surfactants were similar [62].

The size of aggregates formed in aqueous solution was determined by DLS at concentration five times the CMC (as determined by surface tension), at an angle of 173° and at the temperature of 30 °C. This temperature was selected due to the very limited solubility in water of most of the ILs used in this study at 25 °C.

The sizes of the aggregates are given as hydrodynamic diameters D_h, obtained from the Stokes-Einstein equation. Size distributions by intensity measured at 30 °C are presented in Fig. 6. Hydrodynamic diameters, as average of four measurements together with polydispersity index (PDI) data are summarized in Table 5.

DLS measurements showed that studied ILs **1, 2, 4, 5, 7** and **8** self-assembled in water into organized structures. Both size distributions obtained for ILs **1** and **4** at 30 °C were bimodal, indicating the presence of two objects: very small (1,7-2 nm) of low intensity and quite large (ca. 150-180 nm) of significantly higher intensity. The peaks of smaller modes most likely correspond to unaggregated molecules or assemblies of at most two or three molecules, i.e. premicellar aggregates

[64]. The size detected for larger aggregates is, most likely, too big for common spherical surfactants micelles, for which usually D_h does not exceed 20 nm [65]. The structures formed in solution at concentration 5 CMC could be wormlike micelles, vesicles [66] or secondary aggregated clusters of indefinite shape.

The size distributions obtained for compounds **2, 5, 7** and **8** were monomodal. They indicate formation of relatively large aggregates of hydrodynamic diameters in the range of 116-175 nm. This size, as in the case of IL **1** and **4,** corresponds to relatively large aggregates such as vesicles or wormlike micelles. The largest aggregates were observed for ILs **1, 7** and **8**, for which hydrodynamic diameter was above 170 nm.

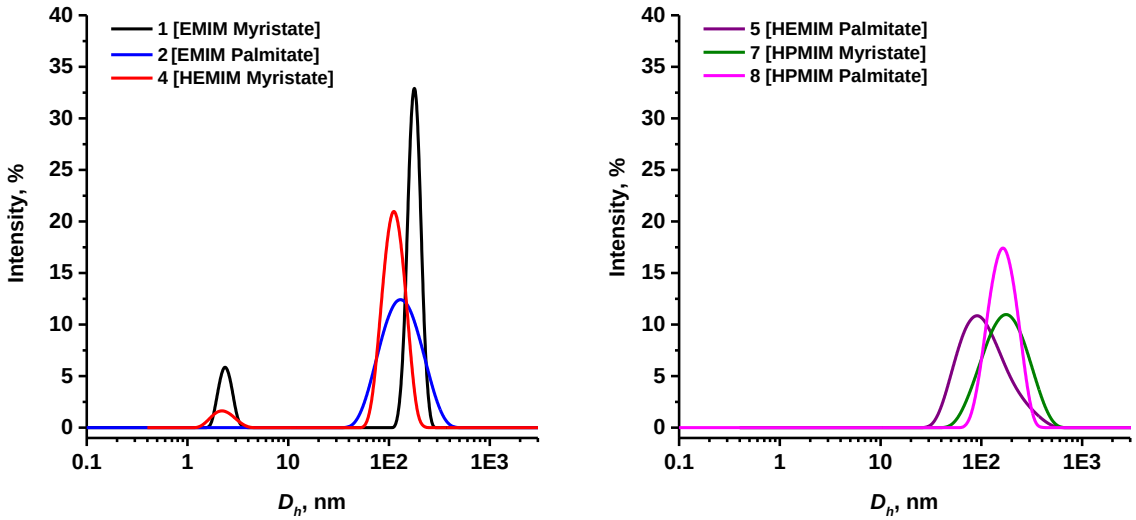

Figure 6. Size distributions by intensity for IL**1, 2, 4, 5, 7, 8** at 30 °C at concentration 5 CMC.

Table 5. The size, dispersity and *ZP* data for ILs water solutions at concentration 5 CMC.

IL	Compound	Temp., °C	D_h, nm	*PDI*	*ZP*, mV
1	**[EMIM Myristate]**	30	1.7; 179	0.46	-73.4
2	**[EMIM Palmitate]**	30	139	0.22	-70.4
4	**[HEMIM Myristate]**	30	2.0; 150	0.36	-72.0
5	**[HEMIM Palmitate]**	30	116	0.37	-96.1
7	**[HPMIM Myristate]**	30	175	0.33	-69.0
8	**[HPMIM Palmitate]**	30	174	0.35	-73.0

The aggregates composed of ILs with myristate [C14] anions (compounds **1, 4, 7**) were found to be relatively larger than those formed by palmitate [C16] anions (compounds **2, 5, 8**). This observation

corroborates the above mentioned results of degree of ionization, which were higher for aggregates of ILs **1, 4, 7** indicating lower degree of compactness of the aggregate.

Electrokinetic potential (*ZP*) is the potential at the slipping plane of a colloid particle moving under electric field [67]. *ZP* provides information about electrostatic repulsion between particles and can be related to the stability of the aggregates formed by the studied ILs in water. According to literature [68], for *ZP* higher than ± 30 mV, colloidal particles are considered to be highly stable. However, *ZP* gives an insight into electrostatic forces, but does not shed light on other interactions, which could contribute to colloid stability, such as van der Walls forces or the impact of steric hindrance.

ZPs of the aggregates formed in solution at concentration 5 CMC and 30 °C are given in Table 5. The assemblies of compounds **1, 2, 4, 5, 7** and **8** were characterized by *ZP* higher than ± 30 mV, which indicates good stability under the conditions employed.

In addition, the thermodynamics of the IL's aggregates formation was determined by isothermal titration calorimetry (ITC). Results of the ITC experiments for [HEMIM Palmitate **2**] are presented in Figure 7, as an example. Enthalpograms were obtained by titration of a concentrated IL solution in the reaction cell containing water, followed by integration of the peaks and normalization with respect to the injected number of moles of IL. The obtained typical sigmoidal shaped enthalpograms represent three different concentration regions, thus three distinct phenomena occurring in the reaction cell.

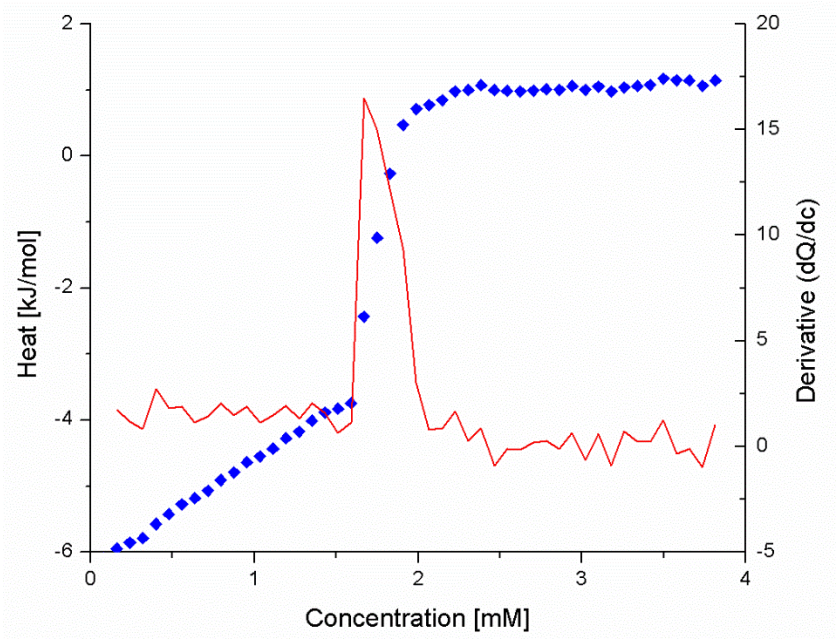

Figure 7. Enthalpogram of ITC titration of [HEMIM Palmitate **2**] aqueous solution at concentration of 15.21 mmol/L into water, first derivative indicates the CMC value

The first step (pre-micellar region) is related to the titration of the concentrated fatty acid IL solution to water. The enthalpic effect consists of heat of micelle dilution, demicellization and dilution of monomers in water. As a next step, a sharp increase of the heat effect due to reaching CMC by IL was detected. Finally, in a post-micellar region, the thermal effect of the titration of the concentrated IL solution to the solution of aggregates is detected. Therefore, no changes in heat effect were observed. To determine the CMC values, the first derivative of the integrated peaks versus the total concentration of fatty acid IL (dQ/dc) was calculated (as shown in Figure 7). In order to determine the enthalpy of demicellization (ΔH_{dem}), the difference between the two horizontal parts of the S-shaped curve representing the pre-micellar and post-micellar regions was calculated. Since during the ITC experiments the concentrated fatty acid IL solution was titrated into water, the observed results reflect a demicellization process, which is the same as the micellization but with an opposite sign. The results of CMC, enthalpy of fatty acid ILs aggregation in aqueous solution, calculated Gibbs energy (equation 1. 4) and entropy of aggregation (equation 1. 5) are collected in Table 6.

Table 6. Thermodynamic parameters of aggregation of long chain fatty acid ILs in water determined at 25 °C

IL	Compound	CMC, mM	ΔG_m, kJ/mol	ΔH_m, kJ/mol	$T\Delta S_m$, kJ/mol
1	**[EMIM Myristate]**	4.7	-36.0	6.3	42.3
2	**[EMIM Palmitate]**	1.5	-44.3	5.1	49.4
4	**[HEMIM Myristate]**	5.5	-34.3	7.2	41.5
5	**[HEMIM Palmitate]**	1.7	-43.5	4.7	48.2
7	**[HPMIM Myristate]**	5.6	-33.1	7.8	40.9
8	**[HPMIM Palmitate]**	1.8	-42.8	4.9	47.7

Two aspects were also considered in the analysis of the thermodynamic results, one related to the chain length of the anion and the other one to the presence of the hydroxyl group in the alkyl chain of the imidazolium cation. All of the micellization processes analyzed at 25 °C were found to be endothermic with the heat effect being lower for palmitate [C16] ILs (4.7-5.1 kJ/mol) in comparison with myristate [C14] derivatives (6.3-7.8 kJ/mol). These relatively high ΔH_m values may be explained by the low solubility of the hydrocarbon substituents, which are present in both cation and anion of ILs and means a high enthalpy of solution [69].

The free energy of micelle formation, ΔG_m, reflecting spontaneity of the system to self-assembly, became more negative for amphiphiles with longer hydrocarbon chain length. This is in agreement

with lower CMC values for palmitate [C16] ILs. The standard free energy of micellization was found to be more negative by about 4 kJ per methylene group. Incorporation of the hydroxyl group in the imidazolium counterion resulted in a slight increase of both ΔH_m and ΔG_m. The obtained data indicated also that negative values of ΔG_m are mainly due to positive entropy, presented in Table 6 as $T\Delta S_m$. Increase of the alkyl chain length resulted in an increase in the value of $T\Delta S_m$. In this regard, the entropy increase on aggregation seems to be the driving force for the process, and is related to a transfer of the hydrophobic alkyl chain of the IL from aqueous solution to the interior of the micelle.

4. Conclusions

Nine fatty acid-based ILs, bearing imidazolium cations with and without hydroxyl groups as substituents, were prepared and characterized to allow for their further exploitation in different applications. All the ILs displayed a complex thermal behavior characterized by different (sometimes overlapping) thermal events. Only the crystallization during the cooling run allowed for a comparison between these structures; an increase of the temperature of this transition was observed as a function of the anion length. As for the thermal stability, the hydroxyl-functionalized EMIM ILs (**4**-**9**) showed practically the same stability, about 20 °C higher than the EMIM ILs **1**-**3**. A similar effect of the hydroxyl group on the stability of carboxylate ILs has been previously reported. Myristate (**1**, **4**, **7**) and palmitate (**2**, **5**, **8**) ILs were able to form aggregates in water and the CMC values were determined by means of surface tension, conductivity measurements, and isothermal titration calorimetry. A good agreement between the CMC values obtained by these three methods was observed. It was found that the increase of the length of the anion alkyl chain has a beneficial effect on the CMC values, and the highest ability to form aggregates was obtained for EMIM palmitate **2**.

Dimensions of the aggregates formed, as a result of DLS measurements, are more consistent with wormlike micelles or vesicles, than common spherical micelles. These aggregates displayed good stability (*ZP* higher than ± 30 mV) and in the case of palmitate ILs (**2**, **5**, **8**) are characterized by a higher degree of compactness.

The micellization processes, and especially for palmitate ILs, were found to be endothermic while the free energy of micelle formation became more negative when the length of the anion was increased, which justifies the lower CMC values of palmitate ILs.

Acknowledgements

The present work has been partially funded by PRA_2018_18 (University of Pisa).

Appendix A. Supplementary data

Supplementary data to this article ca be found online at

References

[1] T. Welton, Ionic liquids: a brief history. Biophys. Rev. 10 (2018), 691-706.

[2] S. Aparicio, M. Atilhan, F. Karadas, Thermophysical Properties of Pure Ionic Liquids: Review of Present Situation. Ind. Eng. Chem. Res. 49 (2010), 9580-9595.

[3] P. G. Jessop., Fundamental properties and practical applications of ionic liquids: concluding remarks. Faraday discuss. 206 (2018), 587-601.

[4] S.P.F. Costa, A.M.O. Azevedo, P.C.A.G. Pinto, M.L.M.F.S. Saraiva, Environmental Impact of Ionic Liquids :Recent Advances in (Eco)toxicology and (Bio)degradability. ChemSusChem, 10 (2017), 2321-2347.

[5] B. Karimi, M. Tavakolian, M. Akbari, F. Mansouri Ionic Liquids in Asymmetric Synthesis: An Overall View from Reaction Media to Supported Ionic Liquid Catalysis. ChemCatChem 10 (2018), 3173-3205.

[6] M. Isik, H. Sardon, D. Mecerreyes, Ionic Liquids and Cellulose: Dissolution, Chemical Modification and Preparation of New Cellulosic Materials. Int. J. Mol. Sci. 15 (2014), 11922-11940.

[7] I. Palazzo, A. Mezzetta, L. Guazzelli, S. Sartini, C.S. Pomelli, W.O. Jr Parker. C. Chiappe, Chiral ionic liquids supported on natural sporopollenin microcapsules, RSC Adv. 8 (2018), 21174-21183.

[8] A. Xu, Y. Zhang, W. Lu, K. Yao, H. Xu, Effect of alkyl chain length in anion on dissolution of cellulose in 1-butyl-3-methylimidazolium carboxylate ionic liquids. J. Mol. Liq. 197 (2014), 211-214.

[9] S. Becherini, A. Mezzetta, C. Chiappe, L. Guazzelli, Levulinate amidinium protic ionic liquids (PILs) as suitable media for the dissolution and levulination of cellulose. New J. Chem. 43 (2019), 4554-4561.

[10] A. Xu, X. Guo, Y. Zhang, Z. Li, J. Wang, Efficient and sustainable solvents for lignin dissolution: aqueous choline carboxylate solutions. Green Chem. 19 (2017), 4067-4073.

[11] C. Chiappe, M.J. Rodriguez Douton, A. Mezzetta, L. Guazzelli, C.S. Pomelli, G. Assanelli, A.R. De Angelis, Exploring and exploiting different catalytic systems for the direct conversion of cellulose into levulinic acid. New J. Chem. 42 (2018), 1845–1852.

[12] A. Xu, L. Chen, J. Wang, Functionalized Imidazalium Carboxylates for Enhancing Practical Applicability in Cellulose Processing. Macromolecules 51 (2018), 4158-4166.
[13] C. Jehanno, M. M. Pérez-Madrigal, J. Demarteau, H. Sardon, A. P. Dove, Organocatalysis for depolymerisation. Polym. Chem. 10 (2019), 172-186.
[14] Q. Yang, Z. Zhang, X.-G. Sun, Y.-S. Hu, H. Xing, S. Dai, Ionic liquids and derived materials for lithium and sodium batteries. Chem. Soc. Rev. 47 (2018), 2020-2064.
[15] F. Ghorbanizamani, S. Timur, Ionic liquids from biocompatibility and electrochemical aspects towards applying in biosensing devices. Anal. Chem. 90 (2018), 640-648.
[16] M. Longhi, S. Arnaboldi, E. Husanu, S. Grecchi, I.F. Buzzi, R. Cirilli, S. Rizzo, C Chiappe, P.R. Mussini, L. Guazzelli, A family of chiral ionic liquids from the natural pool: relationships between structure and functional properties and electrochemical enantiodiscrimination tests, Electrochim. Acta 298 (2019), 194–209.
[17] A.Zajac, R. Kukawka, A. Pawlowska-Zygarowicz, O. Stolarska, M. Smiglak, Ionic liquids as bioactive chemical tools for use in agriculture and the preservation of agricultural products. Green Chem. 20 (2018), 4764-4789.
[18] J. Pernak, B. Łęgosz, T. Klejdysz, K. Marcinkowska, J. Rogowski, D. Kurasiak-Popowska, K. Stuper-Szablewska, Ammonium bio-ionic liquids based on camelina oil as potential novel agrochemicals. RSC Adv. 8 (2018), 28676-28683.
[19] S. Tang, G.A. Baker, H. Zhao, Ether- and alcohol- functionalized task-specific ionic liquids: attractive properties and applications. Chem. Soc. Rev. 41 (2012), 4030-4066.
[20] V.F. Scalfani, A.A. Alshaikh AA, J.E. Bara, Analysis of the frequency and diversity of 1,3-dialkylimidazolium ionic liquids appearing in the literature. Ind. Eng. Chem. Res. 47 (2018), 15971-15981.
[21] P. Drucker, A. Ruhling, D.Grill, D. Wang, A. Draeger, V. Gerke, F. Glorius, H.J. Galla, Imidazolium salts mimicking the structure of natural lipids exploit remarkable properties forming lamellar phases and giant vesicles, Langmuir 33 (2017), 1333−1342.
[22] C. Jungnickel, J. Luczak, J. Ranke, J.F. Fernandez, A. Muller, J. Thoming, Micelle formation of imidazolium ionic liquids in aqueous solution, Colloid. Surface. A 316 (2008), 278-284.
[23] S. Mandal, J. Kuchlyan, D. Banik, S. Ghosh, C. Banerjee, V. Khorwal, N. Sarkar, Ultrafast FRET to Study Spontaneous Micelle-to-Vesicle Transitions in an Aqueous Mixed Surface-Active Ionic-Liquid System, ChemPhysChem 15 (2014), 3544 – 3553.
[24] M. T. Garcia, I. Ribosa, L. Perez, A. Manresa, F. Comelles, Aggregation behavior and antimicrobial activity of ester-functionalized imidazolium-and pyridinium-based ionic liquids in aqueous solution. Langmuir 29 (2013), 2536−2545.

[25] J. Łuczak, C. Jungnickel, I. Łącka, S. Stolte, J. Hupka, Antimicrobial and surface activity of 1-alkyl-3-methylimidazolium derivatives, Green Chem., 12 (2010), 593–601.

[26] J. Łuczak, C. Jungnickel, M. Joskowska, J. Thöming, J. Hupka Thermodynamics of micellization of imidazolium ionic liquids in aqueous solutions, J. Colloid Interf. Sci. 336 (2009) 111–116

[27] J. Łuczak, M. Markiewicz, J. Thöming, J. Hupka, C. Jungnickel, Influence of the Hofmeister anions on self-organization of 1-decyl-3-methylimidazolium chloride in aqueous solutions, J. Colloid Interf. Sci. 362 (2011) 415–422.

[28] J. Łuczak, J. Hupka, J. Thöming, C. Jungnickel. Self-organization of imidazolium ionic liquids in aqueous solution, Colloid. Surface. A, 329 (2008) 125–133

[29] P. Setua, R. Pramanik, S. Sarkar, C. Ghatak, V. G. Rao, N. Sarkar, S. K. Das, Synthesis of silver nanoparticle in imidazolium and pyrolidium based ionic liquid reverse micelles: A step forward in nanostructure inorganic material in room temperature ionic liquid field, J. Mol. Liq. 162 (2011) 33-37.

[30] J. Nowicki, J. Woch, J. Łuczak, M. Zarebska, E. Nowakowska-Bogdan, M. Mościpan, Micellar Route of the Synthesis of Alkyl Xylosides: An Unexpected Effect of Amphiphilic Imidazolium Ionic Liquids. ChemistrySelect 3 (2018), 5254-5262.

[31] J. Nowicki, J. Woch, J. Łuczak, E. Nowakowska-Bogdan, M. Mościpan, Micellar Route of the Synthesis of Alkyl Xylosides: An Unexpected Effect of Amphiphilic Imidazolium Ionic Liquids, ChemistrySelect 3 (19), 5254-5262

[32] I. Svinyarov, M.G. Bogdanov, Ionic liquid-assisted micellar extraction for the quantitative determination of sesquiterpenic acids in *Valeriana officinalis L.* (Caprifoliaceae), Separ. Sci. Technol., 53 (2018), 1230-1240.

[33] F.A.E. Torres, A.C. de Almeida Francisco, J.F.B. Pereira, V.D.C. Santos-Ebinuma, Imidazolium-based ionic liquids as co-surfactants in aqueous micellar two-phase systems composed of nonionic surfactants and their aptitude for recovery of natural colorants from fermented broth, Sep. Purif. Technol. 196 (2018) 262-269

[34] S. Mahajan, R. Sharma, R. K. Mahajan, An investigation of drug binding ability of a surface active ionic liquid: micellization, electrochemical, and spectroscopic studies. Langmuir 28 (2012), 17238−17246.

[35] D. Wang, C. Richter, A. Ruhling, P. Drucker, D. Siegmund, N. Metzler-Nolte, F. Glorius, H. J. Galla, A Remarkably Simple Class of Imidazolium-Based Lipids and Their Biological Properties. Chem. Eur. J. 21 (2015), 15123−15126.

[36] J. Hulsbosch, D.E. De Vos, K. Binnemans, R. Ameloot, Biobased Ionic Liquids: Solvents for a Green Processing Industry? ACS Sustain. Chem. Eng. 4 (2016), 2917-2931.

[37] A. Mezzetta, L. Guazzelli, M. Seggiani, C.S. Pomelli, M. Puccini, C. Chiappe, A general environmentally friendly access to long chain fatty acid ionic liquids (LCFA-ILs), Green Chem. 19 (2017), 3103-3111.

[38] S.M.T. Raes, L. Jourdin, L. Carlucci, A. vann den Bruinhorst, D.P.B.T.B. Strik, C.J.N. Buisman, Water-Based Synthesis of Hydrophobic Ionic Liquids $[N_{8888}]$[oleate] and $[P_{666,14}]$[oleate] and their Bioprocess Compatibility. ChemistryOpen 7 (2018), 878-884.

[39] S. Duan, Y. Jiang, T. Geng, H. Ju, Y. Wang, Methyltriphenylphosphonium carboxylate ionic liquids: Green synthesis, adsorption and aggregation behavior in aqueous solution. J. Disper. Sci. Technol. (2019), DOI: 10.1080/01932691.2018.1561300.

[40] M. Fan, L. Ma, C. Zhang, Z. Wang, J. Ruan, M. Han, Y. Ren, C. Zhang, D. Yang, F. Zhou, W. Liu, Biobased green lubricants: physiochemical, tribological properties of fatty acid ionic liquids. Tribol. T. 61 (2018), 195-206.

[41] R. Gusain, S. Dhingra, O.P. Khatri, Fatty-acid-constituted halogen-free ionic liquids as renewable, environmentally friendly, and high-performance lubricant additives. Ind. Eng. Chem. Res. 55 (2016), 856-865.

[42] R. Gusain, O.P. Khatri, Fatty acid ionic liquids as environmentally friendly lubricants for low friction and wear. RSC Adv. 6 (2016), 3462-3469.

[43] Y. Huang, T. Ke, Y. Ke, Q. Ren, Q. Yang, H. Xing, Carboxylate ionic liquids with large free volume and strong hydrogen bonding basicity for efficient separation of butadiene and n-butene. Ind. Eng. Chem. Res. 57 (2018), 13519-13527.

[44] A.A.C.T. Hijo, G.J. Maximo, M.C. Costa, R.L. Cunha, J.F.B. Pereira, K.A. Kurnia, E.A.C. Batista, A.J.A. Meirelles, Phase behavior and phase properties of new bio-based ionic liquid crystals. J. Phys. Chem. B 121 (2017), 3177-3189.

[45] N. Kundu, P. Banerjee, S. Kundu, R. Dutta, N. Sarkar, Sodium Chloride Triggered the Fusion of Vesicle Composed of Fatty Acid Modified Protic Ionic Liquid: A New Insight into the Membrane Fusion Monitored through Fluorescence Lifetime Imaging Microscopy. J. Phys. Chem. B 121 (2017), 24-34.

[46] A.A.C.T. Hijo, G.J. Maximo, R.L. Cunha, F.H.S. Fonseca, L.P. Cardoso, J.F.B. Pereira, M.C. Costa, E.A.C. Batista, A.J.A. Meirelles, Phase equilibrium and physical properties of biobased ionic liquids mixtures. Phys. Chem. Chem. Phys. 20 (2018), 6469-6479.

[47] S. Duan, Y. Jiang, T. Geng, H. Ju, Y. Wang, Wetting, foaming, and emulsification properties of novel methyltriphenylphosphonium carboxylate ionic liquid surfactants. J. Disper. Sci. Technol. (2019) DOI: 10.1080/01932691.2018.1541416.

[48] Y. Dong, J. Holm, J. Karkkainen, J. Nowicki, U. Lassi, Dissolution and hydrolysis of fibre sludge using hydroxyalkylimidazolium hydrogensulphate ionic liquids. Biomass Bioenerg. 70 (2014) 461-467.

[49] L. Guglielmero, A. Mezzetta, L. Guazzelli, C.S. Pomelli, F. D'Andrea, C. Chiappe. Systematic synthesis and properties evaluation of dicationic ionic liquids, and a glance into a potential new field, Front. Chem. 6 (2018), 612.

[50] R.K. Seddon, A. Stark, M.-J. Torres, Influence of Chloride, Water, and Organic Solvents on the Physical Properties of Ionic Liquids. Pure Appl. Chem. 72 (2000), 2275-87.

[51] C Maton, N. De Vos , C.V. Stevens, Ionic liquid thermal stabilities: decomposition mechanisms and analysis tools. Chem. Soc. Rev. 42 (2013), 5963–77.

[52] Y. Cao, T. Mu, Comprehensive Investigation on the Thermal Stability of 66 Ionic Liquids by Thermogravimetric Analysis. Ind. Eng. Chem. Res. 53 (2014), 8651-8664.

[53] M. Villanueva, A. Coronas, J. García, J. Salgado, Thermal Stability of Ionic Liquids for Their Application as New Absorbents. Ind. Eng. Chem. Res. 52 (2013), 15718−15727.

[54] Y. Song, Y. Xia, Z. Liu, Influence of cation structure on physicochemical and antiwear properties of hydroxyl-functionalized imidazolium bis(trifluoromethylsulfonyl)imide ionic liquids. Tribol. T, 55 (2012), 738-746.

[55] E. Gómez, N. Calvarn, A. Domínguez, Thermal Behaviour of Pure Ionic Liquids Scott Handy, IntechOpen, (2015), Chapter 8, 199-228.

[56] M.A.A. Rocha, A. van der Bruinhorst, W. Schöer, B. Rathke, M.C. Kroon, Physicochemical properties of fatty acid based ionic liquids. J. Chem. Thermodyn. 100 (2016), 156-164.

[57] M. Biswas, M. Dule, P.N. Samanta, S. Ghosh, T.K. Mandal, Imidazolium-based ionic liquids with different fatty acid anions: phase behavior, electronic structure and ionic conductivity investigation. Phys. Chem. Chem. Phys. 16 (2014), 16255-16263.

[58] P. Somasundaran, Reagents in mineral technology, Marcel Dekker, Inc., (1988).

[59] M.S. Akhter, Effect of acetamide on the critical micelle concentration of aqueous solutions of some surfactants. Colloid. Surface. A 121 (1997), 103-109.

[60] F. Geng, J. Liu, L. Zheng, L. Yu, Z. Li, G. Li, C.Tung, Micelle Formation of Long-Chain Imidazolium Ionic Liquids in Aqueous Solution Measured by Isothermal Titration Microcalorimetry. J. Chem. Eng. Data 55 (2010), 147–151.

[61] Y. Wei, F. Wang, Z. Zhang, C. Ren, and Y. Lin, Micellization and Thermodynamic Study of 1-Alkyl-3-methylimidazolium Tetrafluoroborate Ionic Liquids in Aqueous Solution. J. Chem. Eng. Data 59 (2014), 1120-1129.

[62] Rosen, M., Surfactants and Interfacial Phenomena. 3th Edition, John Wiley & Sons, (2004).

[63] H. Ma, H. Ke, T. Wang, J. Xiao, N. Du, L. Yu, Self-assembly of imidazolium-based surface active ionic liquids in aqueous solution: The role of different substituent group on aromatic counterions. J. Mol. Liq. 240, (2017), 556-563.

[64] R. Hadgiivanova, H. Diamant, Premicellar Aggregation of Amphiphilic Molecules. J. Phys. Chem. B. 30 (2007), 8854-8859.

[65] N. J. Buurma, Kinetic medium effects on organic reactions in aqueous colloidal solutions, 43, J. P. B. T.-A. P. O. C. Richard, Ed. Academic Press, (2009), 1–37.

[66] J. Woch, J. Iłowska, Z. Hordyjewicz-Baran, S. Arabasz, B. Kaczmarczyk, R. Grabowski, M. Libera, A. Dworak, B. Trzebicka, Aqueous solution behaviour and solubilisation properties of octadecyl cationic gemini surfactants and their comparison with their amide gemini analogues. Soft Matter. 14 (2018), 754-764.

[67] M. Kaszuba, J. Corbett, F.M. Watson, A. Jones, Philos, High-concentration zeta potential measurements using light-scattering techniques. Philos. T. Roy. Soc. A. 368 (2010), 4439-4451.

[68] S. Bhattacharjee, DLS and zeta potential - What they are and what they are not?. J. Control. Rel. 235 (2016), 337–351.

[69] J. Eastoe, Colloid Science Principles, Methods and Applications, Blackwell Publishing (2005) Chapter 4.